



HAL
open science

Mechanochemical synthesis and study of the local structure of NaGaS₂ glass and glass-ceramics

Louisiane Verger, Julien Trébosc, Benoît Baptiste, Eric Furet, Killian Dénoue, Jiajie Zhang, François Cheviré, David Le Coq, Laurent Calvez, Olivier Lafon, et al.

► **To cite this version:**

Louisiane Verger, Julien Trébosc, Benoît Baptiste, Eric Furet, Killian Dénoue, et al.. Mechanochemical synthesis and study of the local structure of NaGaS₂ glass and glass-ceramics. *Inorganic Chemistry*, 2022, 61 (46), pp.18476-18485. 10.1021/acs.inorgchem.2c02708 . hal-03833401

HAL Id: hal-03833401

<https://univ-rennes.hal.science/hal-03833401>

Submitted on 8 Nov 2022

HAL is a multi-disciplinary open access archive for the deposit and dissemination of scientific research documents, whether they are published or not. The documents may come from teaching and research institutions in France or abroad, or from public or private research centers.

L'archive ouverte pluridisciplinaire **HAL**, est destinée au dépôt et à la diffusion de documents scientifiques de niveau recherche, publiés ou non, émanant des établissements d'enseignement et de recherche français ou étrangers, des laboratoires publics ou privés.

Mechanochemical synthesis and study of the local structure of NaGaS₂ glass and glass-ceramics

Louisiane Verger*¹, Julien Trébosc², Benoît Baptiste³, Eric Furet¹, Killian Dénoue¹, Jiajie Zhang¹, François Cheviré¹, David Le Coq¹, Laurent Calvez¹, Olivier Lafon⁴, Olivier Hernandez^{1,5}

¹ Univ Rennes, CNRS, ISCR (Institut des Sciences Chimiques de Rennes) – UMR 6226, F-35000 Rennes, France

² Univ. Lille, CNRS, INRAE, Centrale Lille, Univ. Artois, FR 2638 – IMEC – Fédération Chevreul, 59000 Lille, France.

³ Institut de Minéralogie, de Physique des Matériaux et de Cosmochimie (IMPMC), UMR 7590 CNRS-Sorbonne Université-IRD-MNHN, case 115, 4 place Jussieu, 75252 Paris Cedex 5, France.

⁴ Univ. Lille, CNRS, Centrale Lille, Univ. Artois, UMR 8181 – UCCS – Unité de Catalyse et Chimie du Solide, 59000 Lille, France.

⁵ Nantes Université, CNRS, Institut des Matériaux de Nantes Jean Rouxel, IMN, F-44000 Nantes, France

**louisiane.verger@univ-rennes1.fr*

Abstract

NaGaS₂ is a newly discovered compound, that have already shown great promise for a variety of applications due to its layered structure and ion exchange properties. In this work, crystalline NaGaS₂ has been synthesized by an alternative method to what has been previously published, namely by mechanochemistry, either by a direct one-step process, or by a two-step process. In the one-step process, crystalline NaGaS₂ is directly formed by milling sodium sulfide Na₂S and gallium (III) sulfide Ga₂S₃. However, an amorphous material is present in majority together with the crystalline phase. In the two-step process, amorphous NaGaS₂ is firstly obtained by mechanical milling, and then heated above its glass transition temperature to obtain a glass-ceramic mainly composed of crystalline NaGaS₂. For the two-step process, changes of the local atomic-level structure in amorphous NaGaS₂ and after crystallization were analyzed by high-field solid-state nuclear magnetic resonance (NMR) spectroscopy as well as by X-ray total scattering and pair distribution function (PDF) analysis. Based on quantitative analysis on the ²³Na NMR spectra, modifying the annealing treatment can promote the formation of the crystalline phase up to a molar fraction of 83.8 %.

Introduction

Crystallization in glasses gathers a wide interest in the materials science community at all length scales, from the formation of homogeneously distributed nanosized crystals to reinforce mechanical properties¹ to the full crystallization for dense transparent ceramics², for example. Glasses can also be precursors for new crystalline phases. In that prospect, metastable superionic phases have been discovered or stabilized at room temperature from glassy precursors. Two examples are particularly relevant: (i) crystallization of high-temperature cubic Na_3PS_4 crystals³ or (ii) stabilization of metastable $\text{Li}_7\text{P}_3\text{S}_{11}$ ⁴ from amorphous precursors. In both cases, conventional solid-state synthesis fails to obtain these phases. Because of their high ionic conductivities and their mechanically soft properties, sulfide-based materials are promising as solid-state electrolytes for all solid-state batteries.⁵ Research for superionic sodium conductors in the scope of the development of Na-ion solid state batteries foster many studies on these compounds, such as the $\text{Na}_2\text{S}\cdot\text{X}$ pseudo-binaries and $\text{Na}_2\text{S}\cdot\text{X}\cdot\text{Y}$ pseudo-ternaries, with $\text{X} = \text{P}_2\text{S}_5$, GeS_2 , or SiS_2 and $\text{Y} = \text{Ga}_2\text{S}_3$, NaCl , or SnS_2 .^{3,6-10}

In this work, we focus on the 50 Na_2S · 50 Ga_2S_3 composition, or NaGaS_2 , an overlooked compound until two years ago when its synthesis and its structure were reported for the first time by two different groups.^{11,12} Adhikaly *et al.* and Klepov *et al.* synthesized NaGaS_2 crystals using polysulfides flux method, from Ga and Na_2S_4 , or Ga, S and Na_2S , respectively, in silica tube sealed under vacuum and heated at 750 or 650 °C.^{11,12} Crystals were then washed to remove the excess of flux, in dimethylformamide or water. NaGaS_2 is sensitive to moisture as water easily inserts in the interlayer space. However, this process is reversible and an additional step of drying is mandatory to dry NaGaS_2 if washed with water. Based on structural refinement against single crystal X-ray diffraction (XRD) data, NaGaS_2 was found to crystallize in the $C2/c$ space group according to a TlGaSe_2 structure type. The structure is based on Ga_4S_{10} units connected by a bridging S atom, resulting in a layered topology. The Ga_4S_{10} units are composed of two pairs of Ga_2S_7 connected through sharing corners. Na^+ ions are located in the valley formed by the Ga_4S_{10} units, in prisms with triangular basis linked via their base to form chains. One prism on two is facing another prism of the upper plane, turned of 90 °. There are therefore two inequivalent sites for Na.

Although the reported ionic conductivity measured for NaGaS_2 is not high enough for a candidate for solid-state electrolyte ($2.88 \times 10^{-7} \text{ S}\cdot\text{cm}^{-1}$ at room temperature),¹¹ a wide variety of applications could benefit from its combination of properties. Thanks to its trapping properties of water molecules, NaGaS_2 was tested as an adsorbent of water with a selectivity

toward small alcohol molecules.¹¹ Furthermore, its ion exchange properties and exfoliation possibilities are particularly interesting for the exploration of new two-dimensional (2D) sulfide-based materials.¹² NaGaS₂ has a wide transparency in the infrared (IR) range (0.31 to 13.30 μm) and birefringence properties that can be modified by different cation substitutions.¹³ An other polymorph of NaGaS₂ was also predicted, and could be a candidate for high-power laser frequency conversion.¹⁴

The synthesis method of NaGaS₂ reported so far in the literature is a bottleneck for the development of this compound on a larger scale, due to the use of silica tubes and the danger risen by vapors with high sulfur content. As an alternative to solid-state and high temperature synthesis, mechanochemical synthesis gathers a growing interest for several reasons.¹⁵ It is a simple, rapid, no-waste, and energy efficient method. It also offers the possibilities to synthesize materials without solvent or gas and to obtain materials that usually require high temperatures. In the case of glasses, mechanochemical milling can enlarge the amorphous domain compared to the one obtained by conventional melt-quenching technique.¹⁶

Different crystalline compounds have been obtained after annealing the corresponding stoichiometric mechanical milled glass in the Na₂S · P₂S₅ binary (Na₂P₂S₆, Na₃PS₄).^{3,17} In this work, we investigate if the same synthesis strategy could be applied for NaGaS₂, as amorphous x [Na₂S] · (100- x) [Ga₂S₃] compounds were obtained through ball milling in our previous work with Na₂S content ranging from $x = 20$ to 80.¹⁶ We report new methods for synthesizing NaGaS₂ glass-ceramic either indirectly through the crystallization of amorphous NaGaS₂ obtained by mechanical milling or directly at room temperature by mechanochemistry synthesis, depending on the milling conditions. In addition, the local environments of Ga and Na atoms in the glass ceramic and the amorphous compound are investigated by high-field solid-state nuclear magnetic resonance (NMR) spectroscopy and X-ray pair distribution function (PDF). The NMR experimental data obtained on crystalline NaGaS₂ are interpreted thanks to the assistance of quantum chemistry calculations.

2. Experimental

Mechanochemical milling was done using a planetary ball mill Pulverisette 7 (Fritsch). Ga₂S₃ was firstly synthesized according to our previous report.¹⁸ In short, 8 g of stoichiometric mixture of gallium (Neyco, 99.99 %) and sulfur (Strem Chemical Inc., 99.999 %) was ball milled during 4 hours at 400 rpm in a tungsten carbide (WC) vessel (internal volume of 45 mL)

with 10 WC balls (diameter 10 mm). Glass and crystalline NaGaS₂ were obtained either directly by mechanochemical milling (one-step process), or followed by an optional thermal treatment (two-step process). Ga₂S₃ and Na₂S (Alfa Aesar, 95% purity) were hand ground in an agate mortar in a molar ratio of 1:1 and placed into two different types of vessel, zirconia (ZrO₂) or tungsten carbide (WC). The powders were milled following two different procedures summarized in Table 1. All processes were performed in a dry N₂ atmosphere. Procedure 1 was chosen to maximize the stressing energy to obtain an amorphous powder in a limited time, while procedure 2 was selected to get a milder milling procedure.

Table 1: Milling conditions of procedures 1 and 2 using ZrO₂ and WC vessels, respectively.

	Materials (bowls and balls)	Diameter (mm)	Milling speed (rpm)	Powder mass (g)	Balls to powder mass ratio
Procedure 1	ZrO ₂	4	600	5	20:1
Procedure 2	WC	10	400	8	10:1

Samples resulting from milling procedures 1 and 2 will be referred as NaGaS₂-Zr-Xh and NaGaS₂-WC-Xh, respectively. *X* corresponds to the milling time in hour. Characteristic temperatures including glass transition temperature (*T_g*) and crystallization onset temperature (*T_x*) are identified based on differential scanning calorimetry (DSC) curves. For the two-step process, an annealing treatment was performed on powders, compressed under 1.5 t and under vacuum using a conventional uniaxial cold press to obtain a 1 to 1.5 mm thick pellet with a 10 mm diameter. The glass pellets were then heated in a silica tube sealed under vacuum and different temperatures and annealing times were tested: at about *T_g* + 40 °C (335 °C) for 24 h and *T_x* + 35 °C (440 °C) for 1.5 h or 24 h.

A DSC Q20 Thermal Analysis was used to characterize the thermal properties of the synthesized materials. Measurements were performed from room temperature up to 500 °C with a heating rate of 10 °C/min on samples sealed under nitrogen in aluminum crucible.

Conventional XRD measurements were performed on powders after different milling times to follow amorphization and reaction processes on samples protected from air by a Kapton (polyimide) window. Note that two different suppliers provide the Kapton windows and their diffraction halos differ (see **Fig. S1** in Supporting Information (SI)). They were recorded in the 5-90° 2θ range with a 0.0261° step size and a counting time of 400 s/step using a PANalytical X'Pert Pro diffractometer (Bragg-Brentano geometry, Cu-source, Ni-filter, *K_α* radiation, 40 kV, 40 mA, PIXcel 1D detector). XRD data on the powder obtain by the two-step process were

recorded on powdered samples protected from air by a polycarbonate dome, which allows a better airtightness.

The glass-ceramic obtained by heating NaGaS₂-Zr-9h at T_x+35 °C for 1.5 h as well as the glass NaGaS₂-Zr-9h were analyzed by X-ray total scattering in silica glass capillaries with 0.3 mm diameter, using a Bruker AXS D8 Advance diffractometer (Debye-Scherrer geometry, $K\alpha$ Mo-radiation selected by a focusing multilayer mirror, 50 kV, 40 mA, LynxEye HE detector). For the glass-ceramic sample, Le Bail profile refinement using the FullProf program¹⁹ was carried out up to $70^\circ 2\theta$ using the Thompson-Cox-Hastings pseudo-Voigt profile function²⁰ and the Bérar and Baldinozzi asymmetry correction²¹. For both samples, PDF data were extracted from those Mo X-ray total scattering data collected up to $155^\circ 2\theta$ (corresponding to instrumental $Q_{\max} = 17.3 \text{ \AA}^{-1}$, where Q is the magnitude of the scattering vector ($Q = (4\pi\sin\theta)/\lambda$), according to a similar procedure as the one described below.

Total X-ray scattering data were also collected at higher energy at the X-ray diffraction platform of IMPMC (UMR CNRS 7590, Paris, France) on Panalytical Empyrean 2-circle diffractometer equipped with a silver X-ray tube and a photo-multiplier detector, in $\theta - \theta$ transmission geometry. Measurements with Ag $K\alpha$ radiation up to $2\theta = 146^\circ$ allowed to obtain an instrumental $Q_{\max} = 21.7 \text{ \AA}^{-1}$. To minimise the statistical noise level at high Q values (due to the low form factor at high angle), the exposure time used for $2^\circ < 2\theta < 50^\circ$ (25 s per 0.2° step) was doubled for $50^\circ < 2\theta < 90^\circ$ and quadrupled for $90^\circ < 2\theta < 148^\circ$. The same data collection strategy was used for both sample and empty capillary measurements to subtract the contribution of the capillary from the signal.

The PDF $G(r)$ gives the probability of finding a pair of atoms separated by a distance r . It is experimentally obtained from the sine Fourier transform of the scattering function $S(Q)$ ^{22,23} as shown in the following equation:

$$G(r) = \frac{2}{\pi} \int_{Q_{\min}}^{Q_{\max}} Q[S(Q) - 1] \sin(Qr) dQ. \quad (\text{Eq. 1})$$

PDFgetX3 was used to process the experimental powder diffraction intensities to generate the $G(r)$.²⁴ Calculations of PDFs using the NaGaS₂ structural published model were done with PDFgui.²⁵

Scanning Electron Microscopy (SEM) images were obtained on a JEOL JSM-IT 300 microscope using an acceleration voltage of 15 kV.

²³Na and ⁷¹Ga NMR spectra were acquired at a static magnetic field $B_0 = 18.8 \text{ T}$ on a Bruker BioSpin Avance NEO NMR spectrometer. These two quadrupolar nuclei with a nuclear

ground-state spin $I = 3/2$ NMR spectra have moderate gyromagnetic ratio, $\gamma(^{23}\text{Na})/\gamma(^1\text{H}) \approx 0.265$ and $\gamma(^{71}\text{Ga})/\gamma(^1\text{H}) \approx 0.306$, and moderate electric quadrupole moment, eQ , with $Q = 10.4 \text{ fm}^2$ for ^{23}Na and 10.7 fm^2 for ^{71}Ga .²⁶ Furthermore, the natural abundance of ^{23}Na and ^{71}Ga nuclei are 100 and 39.89 %, respectively. To prevent contact with moisture, the NaGaS_2 samples were packed into the rotors inside an argon-filled glovebox. The rotors were spun at a magic-angle spinning (MAS) frequency, $\nu_R = 20 \text{ kHz}$. All the NMR spectra, except those shown in **Fig. S8**, were acquired at around 320 K. For the 1D ^{23}Na MAS NMR spectra in **Fig. S8** acquired at the temperature ranging from 220 to 350 K, the temperature of the sample was regulated using BCU II device. The temperature inside the rotor was calibrated using the ^{207}Pb chemical shift of lead nitrate.²⁷

The spectrum at 320 K were acquired using a 3.2 mm double-resonance HX Bruker probe. Quantitative one-dimensional (1D) ^{23}Na and ^{71}Ga NMR spectra were acquired using Bloch-decay experiment with a pulse length of 1.0 and 0.85 μs , respectively, and a radiofrequency (rf) field strength of 62 and 78 kHz, respectively, corresponding to flip angles of 45° for the pulses selective of the central transition (CT).²⁸ These 1D ^{23}Na and ^{71}Ga spectra result from averaging few hundreds transients with recycle delays of 0.5 to 1 s and were processed without apodization. Their baseline was corrected using cubic splines. Furthermore, two-dimensional (2D) ^{23}Na and ^{71}Ga triple-quantum MAS (3QMAS) spectra were acquired using hypercomplex States-TPPI procedure and the z-filter pulse sequence.²⁹ Excitation and reconversion pulses lasted $\tau_p = 6.5$ and 2 μs with an rf field amplitude $\nu_1 = 98 \text{ kHz}$ for ^{23}Na and $\tau_p = 9.5$ and 2.5 μs with $\nu_1 = 78 \text{ kHz}$ for ^{71}Ga , whereas the pulse selective of the CT lasted $\tau_p = 6.5 \mu\text{s}$ with $\nu_1 = 18 \text{ kHz}$ for ^{23}Na and $\tau_p = 32 \mu\text{s}$ with $\nu_1 = 4 \text{ kHz}$ for ^{71}Ga . The ^{23}Na 3QMAS spectrum resulted from averaging 24 transients for each of 120 t_1 increments with $\Delta t_1 = 50 \mu\text{s}$ and a recycle delay of 1 s, corresponding to a total experimental time of 1 h 35 min, whereas the ^{71}Ga 3QMAS spectrum resulted from averaging 1152 transients for each of 60 t_1 increments with $\Delta t_1 = 50 \mu\text{s}$ and a recycle delay of 0.5 s, corresponding to total experimental time of 2 h 30 to 10 h. The 2D ^{23}Na and ^{71}Ga 3QMAS spectra were processed without apodization. ^{23}Na variable temperature measurements were recorded with similar setup and parameters (pulse length 1 μs , rf field $\sim 80 \text{ kHz}$, recycling delay 1 s, MAS rate 20 kHz) except for the use of a 1.6 mm HX PhoenixNMR probe. The ^1H isotropic chemical shifts were referenced to tetramethylsilane (TMS) using the signal of CH_2 group of adamantane at 1.85 ppm as a secondary reference. ^{23}Na and ^{71}Ga chemical shifts were indirectly referenced using the previously published relative NMR frequencies.²⁶

The quantitative 1D ^{23}Na MAS NMR spectra, including both the CT and the satellite transitions (STs), along with the 2D ^{23}Na 3QMAS spectra without shearing were simulated simultaneously using ssNake software.³⁰ The 1D and 2D spectra were simulated by employing the same distribution of isotropic chemical shift with an average value (δ_{iso}) and a Gaussian full-width at half maximum (FWHM) (W_G) as well as the same parameters for the quadrupolar coupling interaction, including the quadrupolar coupling constant (C_Q) and the asymmetry parameter of the electric field gradient tensor (η_Q), and identical Lorentzian FWHM (W_L) of the CT. Additional simulation parameters included (i) Lorentzian FWHM, distinct from W_L , for the STs of the 1D MAS NMR spectra and the triple-quantum transitions detected along the indirect F_1 dimension of the 2D 3QMAS spectra as well as (ii) integrated intensities of the signals, which differ between 1D MAS and 2D 3QMAS spectra since the excitation of triple-quantum coherences depends on the C_Q value. The integrated intensities of the different signals used to simulate the quantitative 1D ^{23}Na NMR spectra were employed to calculate the fractions of the different Na sites. The 2D ^{71}Ga 3QMAS spectrum of NaGaS₂ glass-ceramics prepared at $T_x + 35$ °C was also simulated using ssNake software.

NMR parameters were computed for the NaGaS₂ crystalline phase, characterized by Adhikary et al.¹¹ Calculations were performed within the Gauge Including Projected Augmented Wave formalism^{31,32} as implemented in the CASTEP program, version 20.³³ We used the PBE exchange and correlation functionals,³⁴ on-the-fly generated ultrasoft pseudopotentials, an expansion of the plane-wave basis sets up to an energy cutoff of 900 eV, and a sampling of the Brillouin zone up to 10×10×8 k -points grid. Tests concerning the convergence of NMR parameters with respect to energy cutoff and k -point sampling are reported in the **Tables S1** and **S2** in SI.

The GIPAW calculations give access to the absolute magnetic shielding tensors (σ). The diagonalization of the symmetric part of these tensors allows to determine their eigenvalues. Using the Haeberlen convention,³⁵ the three eigenvalues can be ordered such as $|\sigma_{zz} - \sigma_{\text{iso}}| \geq |\sigma_{xx} - \sigma_{\text{iso}}| \geq |\sigma_{yy} - \sigma_{\text{iso}}|$, and the NMR parameters including the isotropic magnetic shielding, σ_{iso} , the anisotropic magnetic shielding, σ_{aniso} , and the asymmetry parameter of the shielding tensor, η_{CS} , can be deduced from σ tensor:

$$\sigma_{\text{iso}} = \frac{1}{3}(\sigma_{xx} + \sigma_{yy} + \sigma_{zz}); \sigma_{\text{aniso}} = \sigma_{zz} - \sigma_{\text{iso}}; \eta_{\text{CS}} = \frac{\sigma_{yy} - \sigma_{xx}}{\sigma_{\text{aniso}}} \quad (\text{Eq.2})$$

Isotropic chemical shift may subsequently be evaluated using the relation: $\delta_{\text{iso}} = \sigma_{\text{ref}} - \sigma_{\text{iso}}$ where, σ_{ref} , can be deduced from a GIPAW calculation on a reference compound.

For quadrupolar nuclei, the electric field gradient (efg) tensor, denoted V , can be obtained from an *ab initio* calculation. In its diagonal form, it gives access to three eigenvalues that can be ordered according to the convention: $|V_{zz}| \geq |V_{xx}| \geq |V_{yy}|$, from which, the quadrupolar interaction is frequently described using C_Q and η_Q parameters:

$$C_Q = \frac{eQV_{zz}}{h}; \eta_Q = \frac{V_{xx} - V_{yy}}{V_{zz}}. \quad (\text{Eq.3})$$

where eQ is the nuclear electric quadrupole moment and h the Planck constant.

3. Results and discussion

Glass and glass-ceramic formation

The reaction during milling is followed by XRD measurements acquired on the powder after different milling times. **Fig. 1a** shows the copper-source XRD patterns of the starting mixture of Ga_2S_3 and Na_2S , and milled for different times using procedure 1 in ZrO_2 bowls (see **Table 1**). The diffraction halo between 15 and $25^\circ 2\theta$ is due to the Kapton window used to protect the sample from air (see **Fig. S1** in SI). Na_2S main peaks are no longer detected after only 3 hours of milling, whereas Ga_2S_3 main reflections (100), (002) and (110) indexed using the $P6_3mc$ space group of $\beta\text{-Ga}_2\text{S}_3$ are detected up to 6 h of milling. This difference may stem from the faster amorphization of Na_2S compared to Ga_2S_3 . From 3 h, an additional peak is detected at approximately $26.5^\circ 2\theta$. It does not correspond to Ga_2S_3 or Na_2S , and is attributed to the main peak of NaGaS_2 according to the work of Klepov *et al.* and Adhikary *et al.*^{11,12} After 9 h of milling, the synthesized sample ($\text{NaGaS}_2\text{-Zr-9h}$) exhibits diffraction halos characteristic of amorphous materials. T_g and T_x temperatures of $\text{NaGaS}_2\text{-Zr-9h}$ are determined based on DSC analysis (**Fig. 1b**). They are about 293°C and 403°C ($\pm 5^\circ\text{C}$), respectively, in good agreement with the literature.¹⁶ SEM analysis on $\text{NaGaS}_2\text{-Zr-9h}$ reveal that the powder is composed of aggregates of submicron particles (**Fig. 1c**).

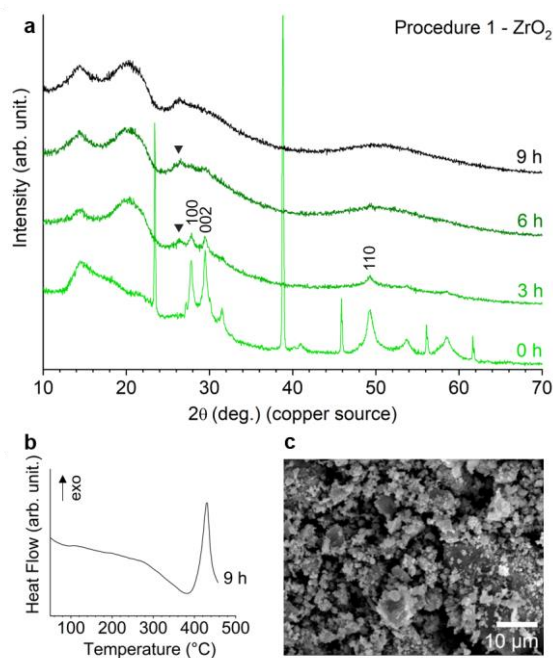


Figure 1: (a) From bottom to top, powder Cu-XRD diagrams of the mixture 50 mol.% Ga_2S_3 and 50 mol.% Na_2S before milling (0 h) and milled for different times (3, 6, and 9 h) in ZrO_2 vessels (procedure 1). Miller indexes correspond to the Ga_2S_3 crystal phase ($P6_3mc$ space group).^{18,36} Peak indexed with a triangle is attributed to crystalline NaGaS_2 .^{11,12} (b) DSC curve of $\text{NaGaS}_2\text{-Zr-9h}$ powdered glass. (c) SEM image of $\text{NaGaS}_2\text{-Zr-9h}$ powdered glass.

Chalcogenide glasses are considered stable against crystallization if the difference of temperature ΔT between T_x and T_g is higher than 100 °C. ΔT of amorphous NaGaS_2 is around 100 °C, as glasses along the binary $\text{Na}_2\text{S}\cdot\text{P}_2\text{S}_5$.³⁷ A pellet of $\text{NaGaS}_2\text{-Zr-9h}$ amorphous powder was heated at about $T_g + 40$ °C (335 °C) for 24 h, a typical annealing treatment to obtain chalcogenide glass-ceramics.¹ **Fig. 2a** shows the Cu-XRD pattern of the resulting material (diagram in the middle, in black). NaGaS_2 is detected as the only crystalline phase. The diffraction halo at 18° 2θ is due to the polycarbonate dome (see **Fig. S1** in SI). No clear difference in the morphology of the particles is observed by SEM before and after crystallization (see **Figs. 1c** and **2c**). When the sample is exposed to air, the structure is greatly affected as water is absorbed in the interlayer space leading to a very clear change of the diffraction pattern. Notably, the 1st Bragg peak is shifted drastically towards lower angles (see top diagram in green in **Fig. 2a**), as expected owing to the fact the monohydrate sample has a larger c parameter by more than 4 Å than the anhydrous one.¹¹

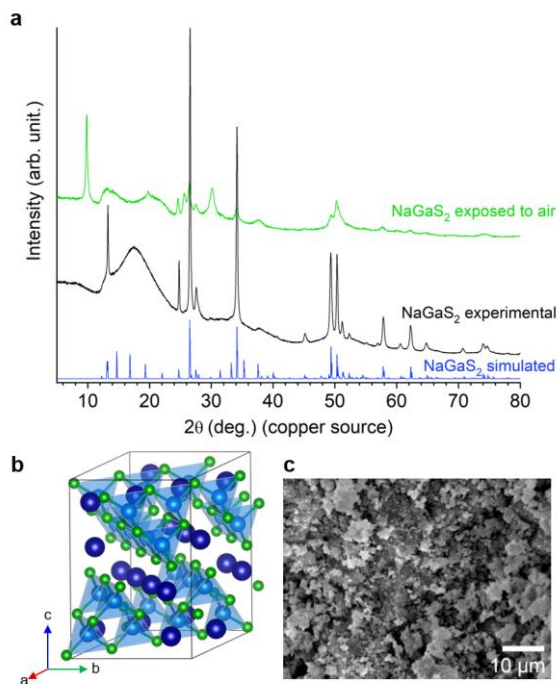


Figure 2: (a) (bottom to top) calculated diffraction pattern of crystalline NaGaS_2 from the structural model of Adhikary *et al.*¹¹ (blue), powder Cu-XRD patterns of the NaGaS_2 glass-ceramic obtained by heating $\text{NaGaS}_2\text{-Zr-9h}$ at $T_g + 40$ °C for 24 h (middle, in black) and after exposure to air (green). (b) Schematic representation of the NaGaS_2 crystal structure. Na, Ga and S atoms are represented in dark blue, light blue and green, respectively. (c) SEM image of the $\text{NaGaS}_2\text{-Zr-9h}$ sample heated at $T_g + 40$ °C for 24 h.

The experimental powder pattern acquired differs significantly from the calculated one (bottom diagram in **Fig. 2a**, in blue) according to Klepov *et al.*¹² and Adhikary *et al.*¹¹ single-crystal structural models, insofar as several calculated peaks are not observed. Possibilities to perform a Rietveld refinement are then extremely limited. Stacking faults in this structure can be quite extensive due to layered structure (**Fig. 2b**), which can greatly affect the intensity and broadening of some reflections leading to apparent observed extinctions. FAULTS program was used to simulate the effect of stacking faults on the XRD pattern.³⁸ The analysis in detail can be found in SI (**Figs S2, S3 and S4**) with the definition of the considered layers. A simple and intuitive stacking fault is a $(\frac{1}{4}, \frac{1}{4}, 0)$ in-plane displacement between two layers. The calculated XRD patterns with various occurrence rate of stacking faults considered are in good agreement with the experimental pattern (**Fig. S4**). A detailed analysis with FAULTS is in progress to perform a Rietveld refinement, considering other possible stacking faults.

Additional annealing treatments on $\text{NaGaS}_2\text{-Zr-9h}$ were tested, from 1.5 h up to 24 h at $T_x + 35$ °C (see **Fig. S5** in SI). They do not result in a better crystallinity of NaGaS_2 , and the stacking

faults observed after 24 h at 335 °C remains predominant. Furthermore, the remaining amount of amorphous phase after the thermal treatment duration cannot be evaluated by XRD since Rietveld refinements are not possible at this stage.

Nevertheless, profile refinement using the Le Bail method without structural constraints was carried out. **Fig. 3** presents the example of NaGaS₂-Zr-9h heated at T_x+35 °C during 1.5 h, using the Mo-XRD pattern acquired in a Debye Scherrer geometry (see experimental section) allowing to minimize preferential orientation. The refined lattice parameters using *C2/c* space group ($a = 10.2144(3)$ Å, $b = 10.2333(3)$ Å, $c = 13.5368(3)$ Å and $\beta = 101.054(2)$) are in good agreement with those reported in the literature.¹¹ Using the instrumental resolution function, the Scherrer formula gives a global average apparent size of diffracting crystallites around 295 Å.

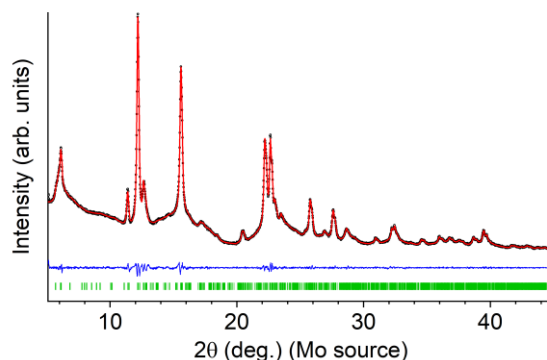


Figure 3: Powder Mo-XRD pattern of the NaGaS₂ glass-ceramic obtained by heating NaGaS₂-Zr-9h at $T_g + 40$ °C for 24 h (black circles) and calculated profile by the Le Bail refinement method ($\chi^2 = 1.60$, $R_{wp} = 7.30\%$, $R_p = 8.47\%$) (red line). The difference is drawn in blue, green bars show the Bragg reflections for NaGaS₂.

In-situ high temperature Cu-XRD measurements were carried out under a nitrogen flow on the NaGaS₂-Zr-9h amorphous powder (see experimental details in SI and **Fig. S6**). The powder remains amorphous until 300 °C and NaGaS₂ starts to crystallize at 400 °C. This composition is then stable under nitrogen and can be simply heated under a controlled atmosphere instead of using evacuated sealed quartz tube. However, the crystallization temperature of NaGaS₂ in the in-situ XRD experiment under nitrogen is higher than the one in evacuated sealed silica tube (335 °C).

To remove the second step of annealing, we investigated the possibility of synthesizing crystalline NaGaS₂ in one step, directly by mechanochemistry. Indeed, using procedure 1, NaGaS₂ is barely detected during milling with the coexistence of the precursor Ga₂S₃. Additional milling time does not promote the formation of crystalline NaGaS₂ but results in an amorphization of the powder (see **Fig. 1a**). To explore the possibility of obtaining NaGaS₂ directly by ball-milling, a milder procedure using WC material was used (procedure 2 in **Table 1**). **Fig. 4** shows the Cu-XRD diagrams acquired on the powder after different milling times according to procedure 2. NaGaS₂ spontaneously appears as in procedure 1 after only 3 h of milling, with un-reacted Ga₂S₃. After 9 h of milling, Ga₂S₃ has almost completely reacted and NaGaS₂ is the only crystalline phase detected. However, the sample remains poorly crystallized, characterized by low intensity and large full width at half-maximum of diffraction peaks. A large amount of amorphous material is also clearly present in the sample. Additional milling time does not improve the crystallinity but rather prolongs the amorphization process as the pattern of NaGaS₂-WC-15h lacks any crystallization peak. Obtaining crystalline NaGaS₂ directly by mechanical milling greatly simplify the synthetic route as it is a one step process. However, further optimization of the milling conditions is required to improve the crystallinity of the sample.

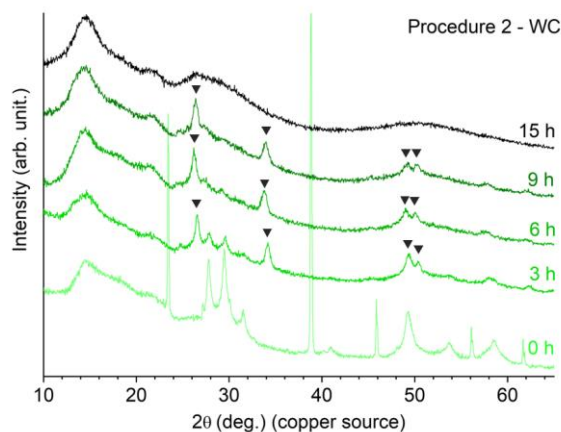


Figure 4: From bottom to top, powder Cu-XRD diagrams of the mixture 50 mol.% Ga₂S₃ and 50 mol.% Na₂S before milling (0 h) and milled for different times (3, 6, 9 and 15 h) in WC vessels (procedure 2). Peaks indexed with a triangle is attributed to crystalline NaGaS₂.^{11,12}

These two new synthesis routes for NaGaS₂ (in one step by mechanical milling or in two steps by heating a mechanical milled glass) offers significant advantages compared to the state of the art. First of all, for annealing at $T_g + 40$ °C (335 °C), the synthesis temperature is lowered

by about 48% and 55% compared to the works of Klepov *et al.* and Adhikary *et al.*, respectively.^{11,12} Furthermore, it is a solvent-free route, providing a material without hydration problem and requiring no additional step of drying. Lastly, a large quantity of material can be synthesized this way, and do not necessarily require the use of silica tubes. Compared to other materials synthesized by a similar synthesis pathway (amorphization by ball-milling followed by thermal annealing at crystallization temperature), the milling time for NaGaS₂, 9 h, is significantly reduced, whereas for example, 20 h were necessary for Na₃PS₄,³ Na₂P₂S₆¹⁷ or Li₇P₃S₁₁.⁴ The drawback of this synthesis routes is that crystalline NaGaS₂ is obtained as a powder. For optical applications, an additional step of shaping is required by using high-temperature isostatic pressure under vacuum, for instance.

Local structure and quantification of the amount of crystalline phase

NMR spectroscopy was used to probe local environments of Na and Ga atoms and to quantify the amount of amorphous phase in the glass-ceramic obtained with one-step (NaGaS₂-WC-9h) and two-step (NaGaS₂-Zr-9h annealed at $T_g + 40$ °C for 24 h, and at $T_x + 35$ °C for 1.5 h or 24 h) methods as it cannot be determined by Rietveld refinement (see above). Furthermore, this technique was also employed to compare the effect of annealing treatment.

The quantitative 1D ²³Na MAS NMR spectra of the investigated samples are displayed on **Fig. 5**. The spectrum of NaGaS₂-Zr-9h only exhibit a broad signal, which indicates a distribution in local ²³Na environments, typical of an amorphous material, in agreement with the XRD pattern shown in **Fig. 1a**. On the contrary, the spectrum of NaGaS₂-WC-9h exhibits an additional narrow signal near -1 ppm assigned to NaGaS₂ crystalline phase in agreement with the XRD pattern of **Fig. 4**. Nevertheless, based on the integrated intensities of the simulated spectrum, we can estimate that the sample is made of 88% of glass phase and only 12% of crystalline phase. Hence, the one-step procedure produces mainly an amorphous phase, even if the crystalline phase is present.

As seen in **Fig. 5b**, the spectrum of NaGaS₂ glass-ceramic sample prepared by annealing of NaGaS₂-Zr-9h at about $T_g + 40$ °C for 24 h exhibits broad signals with $\delta_{iso} = 11.2$ and 4.9 ppm assigned to amorphous NaGaS₂ (see **Table 2**). The two narrow peaks at $\delta_{iso} = -0.3$ and -1.3 ppm are assigned to the Na2 and Na1 sites of NaGaS₂ crystalline phase represented in the crystal structure in **Figs. S3** and **S7** in SI, based on the DFT calculation of ²³Na NMR parameters shown in **Table S1**.^{11,12} The Na1 signal, which is more shielded than Na2, is subject to smaller

quadrupolar interaction since it faces another Na1 atom (see **Fig. S7**) and hence, occupies a more symmetrical local environment. The signals of the two Na sites are better resolved in the 2D ^{23}Na 3QMAS spectrum shown in **Fig. 5c**. The simulation of the quantitative 1D ^{23}Na spectrum of NaGaS₂ glass-ceramic sample annealed at about $T_g + 40$ °C for 24 h indicates that this sample contain 47.5% of crystalline phase and 41.1% of glass phase (see **Table 2**). The remaining integrated intensity (11.4%) is produced mainly by broad signals with isotropic chemical shifts close to the crystalline phase, which could stem from defects of the crystalline phase, such as stacking faults or grain boundaries, or unidentified impurities.

The GIPAW calculations indicate a difference between the chemical shielding values of the two Na sites of the NaGaS₂ phase that is never below 3.1 ppm (500 eV - $5 \times 5 \times 4$ grid), instead of 1 ppm in the spectrum acquired at 320 K. For the costliest calculations (900 eV - $10 \times 10 \times 8$ grid), the difference stabilizes and tops to 3.6 ppm. For the sake of completeness, an additional calculation has been performed by optimizing the atomic positions while keeping the NaGaS₂ cell parameters fixed. Such relaxation process does not lead to a reduction of the difference between the chemical shield values but to a small increase of 0.5 ppm. It seems therefore that our calculations performed at 0 K, cannot reproduce the experimental difference obtained at temperature close to room temperature.

We recorded the quantitative 1D ^{23}Na MAS NMR spectra of NaGaS₂ glass-ceramics annealed at about $T_g + 40$ °C for 24 h at temperature ranging from 220 to 350 K (see **Fig. S8a** in SI). We observe a narrowing of ^{23}Na signal of the amorphous phase at higher temperature in the sample prepared at $T_g + 40$ °C for 24 h. It indicates an increased mobility of Na⁺ cations at higher temperature in the glass (see **Fig. S8a**). Furthermore, the difference between the resonance frequencies of the two ^{23}Na sites of NaGaS₂ crystalline phase decreases at higher temperature since the motions of the Na⁺ cations average out the difference in the local environment of the two Na sites (see **Fig. S8b**). The signals of ^{23}Na sites of NaGaS₂ crystal overlap above 310 K. At 220 K, the difference between the two ^{23}Na sites of NaGaS₂ crystalline phase is about 1.9 ppm. We can expect that at lower temperature, the difference in ^{23}Na isotropic chemical shift will increase further and reach value close to 3.6 ppm calculated by DFT at 0 K.

Annealing at $T_x + 35$ °C for 1.5 h reduces the fraction of the amorphous phase (see **Fig. 5a**) since the signals of the glass at 11 and 5 ppm are no longer visible. According to the simulation of the spectrum in **Fig. S9**, the signals of NaGaS₂ crystalline phase amount to 83.8% of the total integrated intensity of the ^{23}Na spectrum (see **Table 2**). Note that the simulation of ^{23}Na signal

of NaGaS₂ crystalline phase required three contributions for that sample. The central peak at -0.9 ppm stems from the crystallites at the highest temperatures, for which the ^{23}Na signals of the two Na sites overlap (see **Fig. S8**), whereas the external signals (at -0.3 and -1.3 ppm) arise from the crystallites at lower temperatures. Hence, these three signals betrays a distribution of temperature inside the rotor.³⁹ The central signal was not detected for the sample annealed at $T_g + 40$ °C for 24 h because of the slightly difference dependence of ^{23}Na spectra between samples annealed at different temperatures (compare the spectra acquired at 310 K in **Fig. S8b** and **c**).

The 1D ^{23}Na NMR spectrum of the glass-ceramics annealed at $T_x + 35$ °C during 1.5 and 24 h are almost identical (see **Fig. 5a**). Prolonged annealing only slightly broadens the foot of the peak. Such a broadening may stem an increased amount of defects for prolonged annealing treatment. The fraction of the NaGaS₂ crystalline phase remains larger than 80%. The 1D ^{23}Na NMR spectra of this sample at temperature ranging from 220 to 350 K are displayed in **Fig. S8c**. As already observed for the glass-ceramics annealed at $T_g + 40$ °C, the two ^{23}Na signals overlap at high temperature.

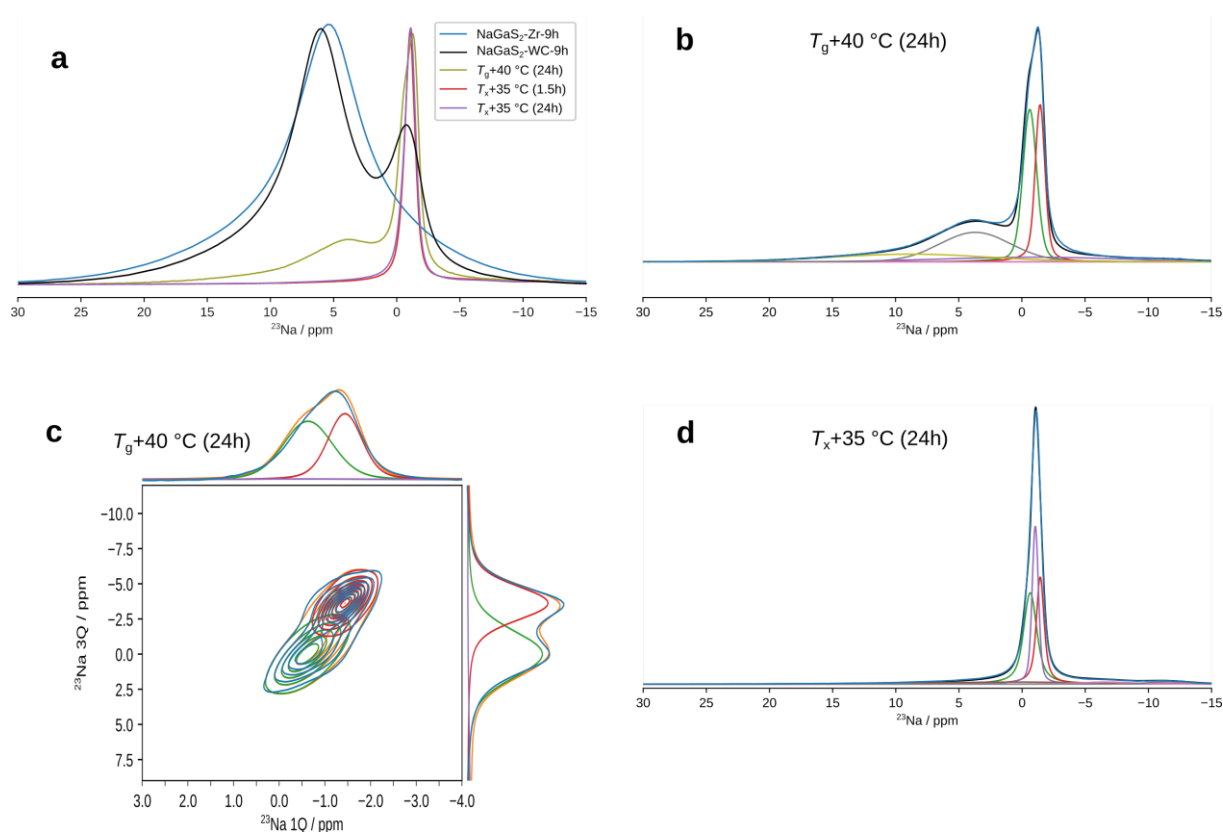


Figure 5: (a) Quantitative 1D ^{23}Na MAS NMR spectra showing CTs of NaGaS₂-Zr-9h (blue), NaGaS₂-WC-9h (black), glass-ceramics obtained by annealing of NaGaS₂-Zr-9h at about $T_g + 40$ °C for 24 h (green), and at $T_x + 35$ °C for 1.5 h (red) or 24 h (purple). (b-d) Experimental and simulated (b,d)

quantitative 1D ^{23}Na MAS and (c) 2D ^{23}Na 3QMAS NMR spectrum without shearing of NaGaS_2 annealed at (b,c) $T_g + 40$ °C for 24 h and (d) $T_x + 35$ °C for 24 h. The experimental 1D NMR spectra in panels b and d are identical to those shown in panel a. Their main best-fit parameters are given in Table 2. This figure only displays the CTs. The experimental and simulated full 1D MAS ^{23}Na spectra of NaGaS_2 annealed at $T_g + 40$ °C and $T_x + 35$ °C for 24 h are shown in **Fig. S10** along with the 2D ^{23}Na 3QMAS NMR spectrum of NaGaS_2 annealed at $T_x + 35$ °C for 24 h. The spectra were acquired at around 320 K.

Table 2: Main parameters of the most intense signals used to simulate ^{23}Na NMR spectra (**Figs. 5, S9 and S10**) of NaGaS_2 glass-ceramics prepared at $T_g + 40$ °C for 24 h, $T_x + 35$ °C for 1.5 h and 24 h. The ^{23}Na signals of NaGaS_2 prepared at $T_g + 40$ °C for 24 h and $T_x + 35$ °C for 24 h were simulated using quadrupolar lineshapes with unique C_Q and η_Q values for each ^{23}Na site.

Sample	Na site	δ_{iso} /ppm	C_Q /MHz	η_Q	W_L /Hz	W_G /ppm	Fraction /% ^a	Fraction attributed to crystalline NaGaS_2 /% ^b
$T_g + 40$ °C for 24 h	-	11.2	2.1	0.1	127	14.0	14.9	/
	-	4.9	1.5	0.1	108	6.2	26.2	/
	Na2	-0.3	0.7	0.25	58	1.1	27.4	47.5
	Na1	-1.3	0.4	0.75	56	0.7	20.1	
$T_x + 35$ °C for 1.5 h	Na2	-0.3	0.7	0.25	109	0.5	28.0	83.8
	Na1,2	-0.9	0.5	1.0	58	0.4	35.3	
	Na1	-1.3	0.4	0.75	77	0.5	20.5	
$T_x + 35$ °C for 24 h	Na2	-0.3	0.7	0.25	99	0.8	31.5	80.3
	Na1,2	-1.0	0.3	0.5	73	0.4	30.0	
	Na1	-1.3	0.4	0.75	48	0.6	18.8	

^a Fraction of the signal integrated intensity for the 1D NMR spectra. ^b Calculated as the sum of the fractions of ^{23}Na signals with $\delta_{\text{iso}} = -0.3, -1.0$ and -1.3 ppm.

Fig. 6a presents the quantitative 1D ^{71}Ga MAS NMR spectra of $\text{NaGaS}_2\text{-Zr-9h}$ before and after annealing. In agreement with its ^{23}Na NMR data, the signal of NaGaS_2 glass is still detected in the spectrum of the sample annealed at $T_g + 40$ °C for 24 h. Conversely, both samples annealed at $T_x + 35$ °C only exhibit the narrow signal of NaGaS_2 crystalline phase. The 2D ^{71}Ga 3QMAS spectrum of NaGaS_2 annealed at $T_x + 35$ °C for 24 h can be simulated by considering two ^{71}Ga sites with close δ_{iso} and C_Q values (**Table 3**), ascribed to the two Ga crystallographic sites of NaGaS_2 crystalline phase, in agreement with the DFT calculation (**Table S2**). Nevertheless, the

experimental and calculated NMR parameters of these two crystallographically inequivalent sites are too close to allow an unambiguous assignment. Whereas ^{23}Na and ^{71}Ga isotopes have similar electric quadrupolar moments, the latter are subject to larger quadrupolar interaction because they are bonded to sulfur atoms.

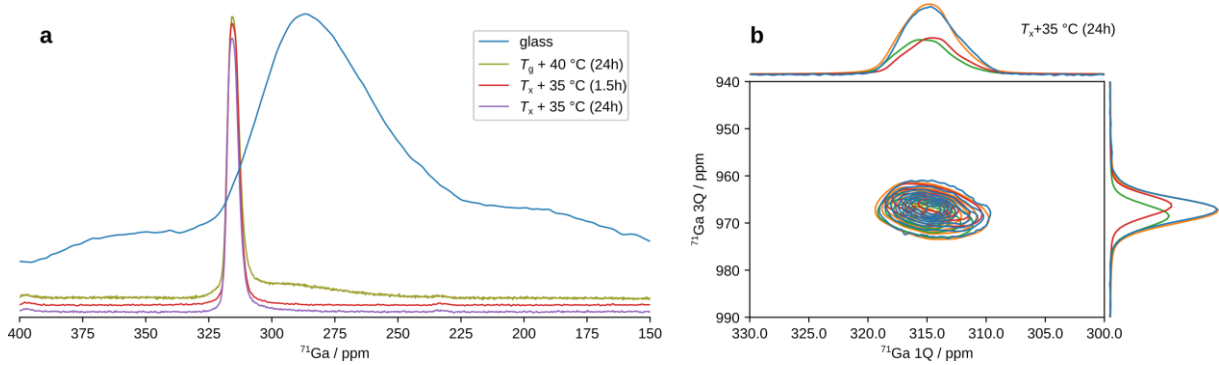


Figure 6: (a) Quantitative 1D ^{71}Ga MAS NMR spectra of $\text{NaGaS}_2\text{-Zr-9h}$ before (blue) and after annealing at about $T_g + 40\text{ }^\circ\text{C}$ for 24 h (green), and at $T_x + 35\text{ }^\circ\text{C}$ for 1.5 h (red) or 24 h (purple). (b) 2D ^{71}Ga 3QMAS spectrum of NaGaS_2 prepared at $T_x + 35\text{ }^\circ\text{C}$ for 24 h.

Table 3: Main parameters used to simulate 2D ^{71}Ga 3QMAS spectrum (shown in **Fig. 6b**) of $\text{NaGaS}_2\text{-Zr-9h}$ annealed at $T_x + 35\text{ }^\circ\text{C}$ for 24 h. The ^{71}Ga signals were simulated using quadrupolar lineshapes with unique C_Q and η_Q values for each ^{71}Ga site.

δ_{iso} /ppm	C_Q /MHz	η_Q	W_L /Hz	W_G /ppm	Fraction /%
318.8	2.82	0.5	224	1.17	50
318.1	2.77	0.6	224	1.06	50

Amorphous versus crystalline structure

To identify the structural modifications between amorphous and crystalline NaGaS_2 phases, X-ray total scattering measurements were performed using two different energies on the $\text{NaGaS}_2\text{-Zr-9h}$ glass, and one of the NaGaS_2 glass-ceramic obtained with the two-step process. Following the NMR analysis, the $\text{NaGaS}_2\text{-Zr-9h}$ heated at $T_x + 35\text{ }^\circ\text{C}$ for 1.5 h glass-ceramic was selected because it contains the larger amount of phase attributed to crystalline NaGaS_2 . The experimental PDFs using Ag radiation (allowing to reach a higher Q_{max} value so leading in principle to the most accurate PDF data) are extracted and represented in **Fig. 7**. We also acquired complementary total scattering data using Mo radiation, and the experimental detail

and PDF can be found in SI, **Figs. S11** and **S12**. The observed PDFs extracted from both experiments are in good adequacy. In the medium range order, above 10 Å, the oscillations of the PDF of the amorphous sample are dominated by termination ripples. A closer look on the short-range order below 7 Å of the amorphous sample highlights both similarities and differences with the glass-ceramic sample (**Fig. 8**). To attribute interatomic distances, the global PDF of NaGaS₂ based on the reported structure of Adhikari *et al.*¹¹ as well as partial PDFs were calculated (see **Fig. S13** in SI)¹¹. As described in the introduction, NaGaS₂ is composed of Ga₄S₁₀ structural units (represented in **Fig. 8**), built from four corner shared GaS₄ tetrahedra.

The first peak (A) on both PDF located at about 2.26-2.27 Å is attributed to Ga-S distances within GaS₄ tetrahedra. The next peak observed in the calculated PDF (see **Fig. S13**) corresponds to Na-S distances, ranging from 2.86 to 3.07 Å. However, this peak is absent from both the observed PDFs (**Fig. 8**). Furthermore, at about 5.1 Å, the Na related peaks (Na-Na, Na-S and Na-Ga distances) are also absent in both samples. This cannot be due to the lower atomic form factor of Na compared to Ga as it is clearly detected in the calculated PDFs. It can be explained by a broadening of the peak due to Na disorder, and/or a decreased intensity due to a decrease of coordination number of Na compared to the crystalline model published. The second intense peak observed in the glass-ceramic can be attributed to two main contributions, Ga-Ga distances (B) (3.58-3.64 Å) and S-S distances (C) within each tetrahedra (3.61 to 3.76 Å) in Ga₄S₁₀ units. In this *r*-region for the glass, the half-height width of the peak is larger than the one for the glass-ceramic, and a splitting is observed involving a shoulder on the right. It indicates a wider distribution of Ga-Ga and S-S distances than in the crystal, and therefore a distortion of the [Ga₄S₁₀] units or an incomplete connection of the GaS₄ tetrahedra to build [Ga₄S₁₀] units. The impact of the value of Q_{max} was tested to check the accuracy of this observed splitting (**Fig. S14**). The splitting is affected when the value of Q_{max} is modified, but the shoulder on the right remains present.

The third and fourth peaks observed in the glass-ceramic are attributed to Ga-S distances at 4.29-4.38 Å (D) and 5.57-5.65 Å (E), respectively, located in the Ga₄S₁₀ tetrahedral structural units. They are represented in **Fig. 8**. These features are absent or at very low intensity in the PDF of the amorphous sample, indicating that this structural unit in the glass is incomplete. Based on these analyses, the presence of edge sharing tetrahedra units in the glass and the glass-ceramics cannot be excluded locally.

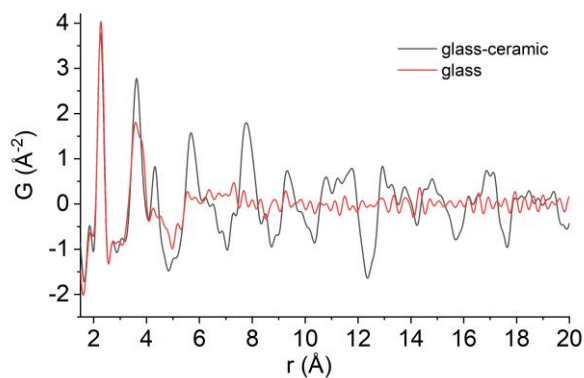


Figure 7: Comparison of observed X-ray PDFs (from data using Ag radiation) of the $\text{NaGaS}_2\text{-Zr-9h}$ amorphous sample (red) and the NaGaS_2 glass-ceramic from the two-step process (annealed at $T_x + 35$ °C for 1.5 h) (black).

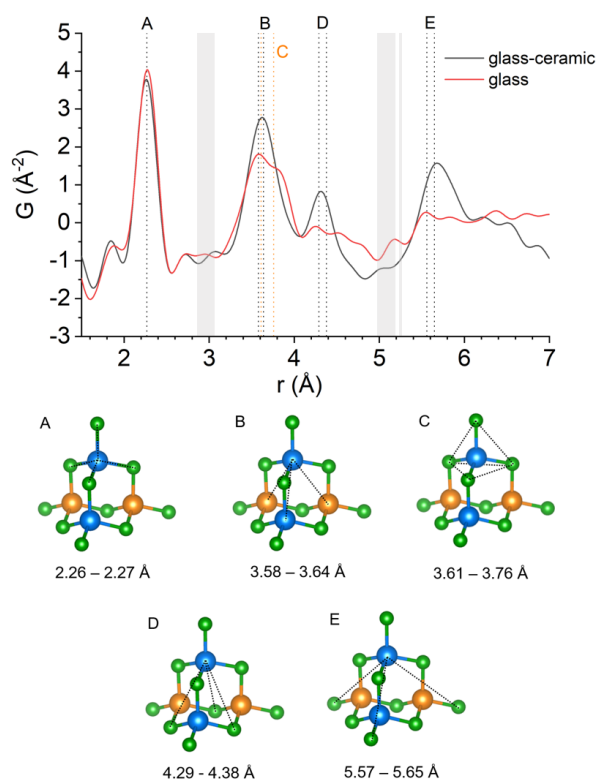


Figure 8: (Top) Observed PDFs (from data using Ag radiation) up to 7 Å of the $\text{NaGaS}_2\text{-Zr-9h}$ amorphous sample (red) and the NaGaS_2 glass-ceramic from the two-step process annealed at $T_x + 35$ °C for 1.5 h (black). The dotted lines correspond to Ga and S related distances based on published reference for NaGaS_2 .¹¹ The shaded gray area corresponds to Na related distances.¹¹ (Bottom) Ga_4S_{10} structural units displaying distances A, B, C, D and E represented for only one Ga atom and/or one GaS_4 tetrahedron for clarity.

Conclusion

Crystalline NaGaS₂ was obtained either directly by mechanochemistry in a one-step process, or after a thermal treatment on a mechanically synthesized glass in a two-step process. Le Bail refinement for the crystallized sample obtained with the two-step process shows good agreement with the reported unit cell of NaGaS₂. Crystallite sizes of 30 nm are proposed for the $T_x + 35$ °C sample according to the analysis of the XRD peak widths. However, possibility to perform Rietveld refinement is limited by the extensive stacking faults observed, whose diffraction features have been however qualitatively reproduced. Local environments in NaGaS₂ glass and glass-ceramics were characterized using laboratory X-ray PDF analysis at two different energies, and ²³Na and ⁷¹Ga solid-state NMR spectroscopy. At short range, both glass and glass-ceramic are composed of GaS₄ tetrahedra. The PDF of the glass-ceramic is as a whole coherent with the reported crystalline structure compatible with the presence of Ga₄S₁₀ structural units composed of corner shared GaS₄ tetrahedra, with the nuance that the Na-related PDF-peaks appear as heavily overdamped. The glass exhibits a wider distribution of Ga-Ga and S-S distances than the crystal. Molecular dynamics calculations are on-going to get a clearer picture of the structure of NaGaS₂ glass. The annealing treatment at higher temperature ($T_x + 35$ °C) on amorphous NaGaS₂ yields to a material mainly composed of crystalline NaGaS₂.

The synthesis strategy already applied for the Na₂S-P₂S₅ system^{17,37} to obtain crystalline phases can therefore also be applied to the Na₂S-Ga₂S₃ binary. This work can certainly be extended to other compositions in the binary, already discovered such as Na₃GaS₃,^{40,41} Na₅GaS₄,⁴² or new phases. Other compositions are being studied, to rationalize the structure of amorphous and crystalline compounds of equal stoichiometry, a key step to improve the ionic conductivity in these systems.

Acknowledgments

This publication is (partially) supported by the European Union through the European Regional Development Fund (ERDF), the Ministry of Higher Education and Research, the French region of Brittany and Rennes Métropole. Financial support from the IR INFRANALYTICS FR2054 for conducting the research is gratefully acknowledged. O.L. and J.L. are grateful for funding provided by the Region Hauts-de-France (France), Europe (FEDER), CNRS, Ministère de l'Enseignement Supérieur et de la Recherche, CPER and Chevreul Institute (FR 2638).

References

- (1) Rozé, M.; Calvez, L.; Ledemi, Y.; Allix, M.; Matzen, G.; Zhang, X.-H. Optical and Mechanical Properties of Glasses and Glass-Ceramics Based on the Ge-Ga-Se System. *J. Am. Ceram. Soc.* **2008**, *91* (11), 3566–3570.
- (2) Allix, M.; Alahrache, S.; Fayon, F.; Suchomel, M.; Porcher, F.; Cardinal, T.; Matzen, G. Highly Transparent BaAl₄O₇ Polycrystalline Ceramic Obtained by Full Crystallization from Glass. *Adv. Mater.* **2012**, *24* (41), 5570–5575.
- (3) Hayashi, A.; Noi, K.; Sakuda, A.; Tatsumisago, M. Superionic Glass-Ceramic Electrolytes for Room-Temperature Rechargeable Sodium Batteries. *Nat. Commun.* **2012**, *3* (1), 856.
- (4) Mizuno, F.; Hayashi, A.; Tadanaga, K.; Tatsumisago, M. New, Highly Ion-Conductive Crystals Precipitated from Li₂S-P₂S₅ Glasses. *Adv. Mater.* **2005**, *17* (7), 918–921.
- (5) Yu, T.; Ke, B.; Li, H.; Guo, S.; Zhou, H. Recent Advances in Sulfide Electrolytes toward High Specific Energy Solid-State Lithium Batteries. *Mater. Chem. Front.* **2021**, *5* (13), 4892–4911.
- (6) Souquet, J. L.; Robinel, E.; Barrau, B.; Ribes, M. Glass Formation and Ionic Conduction in the M₂S-GeS₂ (M = Li, Na, Ag) Systems. *Solid State Ionics* **1981**, *3–4* (C), 317–321.
- (7) Ribes, M.; Barrau, B.; Souquet, J. L. Sulfide Glasses: Glass Forming Region, Structure and Ionic Conduction of Glasses in Na₂S-XS₂ (X=Si; Ge), Na₂S-P₂S₅ and Li₂S-GeS₂ Systems. *J. Non. Cryst. Solids* **1980**, *38–39* (PART 1), 271–276.
- (8) Yao, W.; Berg, K.; Martin, S. Structure and Properties of Glasses in the MI + M₂S + (0.1Ga₂S₃ + 0.9GeS₂), M = Li, Na, K and Cs, System. *J. Non. Cryst. Solids* **2008**, *354* (18), 2045–2053.
- (9) Chu, I. H.; Kompella, C. S.; Nguyen, H.; Zhu, Z.; Hy, S.; Deng, Z.; Meng, Y. S.; Ong, S. P. Room-Temperature All-Solid-State Rechargeable Sodium-Ion Batteries with a Cl-Doped Na₃PS₄ Superionic Conductor. *Sci. Rep.* **2016**, *6* (1), 33733.
- (10) Zhang, Z.; Ramos, E.; Lalère, F.; Assoud, A.; Kaup, K.; Hartman, P.; Nazar, L. F. Na₁₁Sn₂PS₁₂: A New Solid State Sodium Superionic Conductor. *Energy Environ. Sci.* **2018**, *11* (1), 87–93.
- (11) Adhikary, A.; Yaghoobnejad Asl, H.; Sandineni, P.; Balijapelly, S.; Mohapatra, S.; Khatua, S.; Konar, S.; Gerasimchuk, N.; Chernatynskiy, A. V.; Choudhury, A. Unusual Atmospheric Water Trapping and Water Induced Reversible Restacking of 2D Gallium Sulfide Layers in NaGaS₂ Formed by Supertetrahedral Building Unit. *Chem. Mater.* **2020**, *32* (13), 5589–5603.
- (12) Klepov, V. V.; Berseneva, A. A.; Pace, K. A.; Kocevski, V.; Sun, M.; Qiu, P.; Wang, H.; Chen, F.; Besmann, T. M.; Loye, H. NaGaS₂: An Elusive Layered Compound with Dynamic Water Absorption and Wide-Ranging Ion-Exchange Properties. *Angew. Chemie Int. Ed.* **2020**, *59* (27), 10836–10841.
- (13) Yun, Y.; Xie, W.; Yang, Z.; Li, G.; Pan, S. Na⁺/Ag⁺ Substitution Induced Birefringence Enhancement from AgGaS₂ to NaGaS₂. *J. Alloys Compd.* **2022**, *896*, 163093.
- (14) Hou, D.; Nissimagoudar, A. S.; Bian, Q.; Wu, K.; Pan, S.; Li, W.; Yang, Z. Prediction and Characterization of NaGaS₂, A High Thermal Conductivity Mid-Infrared Nonlinear Optical Material for High-Power Laser Frequency Conversion. *Inorg. Chem.* **2019**, *58* (1), 93–98.
- (15) Baláž, P.; Achimovicová, M.; Baláž, M.; Billik, P.; Zara, C. Z.; Criado, J. M.; Delogu, F.; Dutková, E.; Gaffet, E.; Gotor, F. J.; Kumar, R.; Mitov, I.; Rojac, T.; Senna, M.; Streletskii, A.; Krystyna, W. C. Hallmarks of Mechanochemistry: From Nanoparticles to Technology. *Chem. Soc. Rev.* **2013**, *42* (18), 7571–7637.
- (16) Dénoue, K.; Le Coq, D.; Calers, C.; Gautier, A.; Verger, L.; Calvez, L. New Synthesis Route for Glasses and Glass-Ceramics in the Ga₂S₃-Na₂S Binary System. *Mater. Res. Bull.* **2021**, *142*, 111423.

- (17) Fritsch, C.; Hansen, A. L.; Indris, S.; Knapp, M.; Ehrenberg, H. Mechanochemical Synthesis of Amorphous and Crystalline Na₂P₂S₆-Elucidation of Local Structural Changes by X-Ray Total Scattering and NMR. *Dalt. Trans.* **2020**, 49 (5), 1668–1673.
- (18) Dénoue, K.; Cheviré, F.; Calers, C.; Verger, L.; Le Coq, D.; Calvez, L. Mechanochemical Synthesis and Structural Characterization of Gallium Sulfide Ga₂S₃. *J. Solid State Chem.* **2020**, 292, 121743.
- (19) Rodríguez-Carvajal, J. Recent Advances in Magnetic Structure Determination by Neutron Powder Diffraction. *Phys. B Condens. Matter* **1993**, 192 (1–2), 55–69.
- (20) Thompson, P.; Cox, D. E.; Hastings, J. B. Rietveld Refinement of Debye–Scherrer Synchrotron X-Ray Data from Al₂O₃. *J. Appl. Crystallogr.* **1987**, 20 (2), 79–83.
- (21) Berar, J. F.; Baldinozzi, G. Modeling of Line-Shape Asymmetry in Powder Diffraction. *J. Appl. Crystallogr.* **1993**, 26 (pt 1), 128–129.
- (22) Egami, T.; Billinge, S. J. L. *Underneath the Bragg Peaks: Structural Analysis of Complex Materials*; Elsevier, 2003.
- (23) Farrow, C. L.; Billinge, S. J. L. Relationship between the Atomic Pair Distribution Function and Small-Angle Scattering: Implications for Modeling of Nanoparticles. **2009**, 65 (3), 232–239.
- (24) Juhás, P.; Davis, T.; Farrow, C. L.; Billinge, S. J. L. PDFgetX3: A Rapid and Highly Automatable Program for Processing Powder Diffraction Data into Total Scattering Pair Distribution Functions. **2013**, 46 (2), 560–566.
- (25) Farrow, C. L.; Juhas, P.; Liu, J. W.; Bryndin, D.; Božin, E. S.; Bloch, J.; Proffen, T.; Billinge, S. J. L. PDFfit2 and PDFgui: Computer Programs for Studying Nanostructure in Crystals. *J. Phys. Condens. Matter* **2007**, 19 (33), 335219.
- (26) Harris, R. K.; Becker, E. D.; De Menezes, S. M. C.; Goodfellow, R.; Granger, P. NMR Nomenclature: Nuclear Spin Properties and Conventions for Chemical Shifts - IUPAC Recommendations 2001. *Solid State Nucl. Magn. Reson.* **2002**, 22 (4), 458–483.
- (27) Bielecki, A.; Burum, D. P. Temperature Dependence of ²⁰⁷Pb MAS Spectra of Solid Lead Nitrate. An Accurate, Sensitive Thermometer for Variable-Temperature MAS. *J. Magn. Reson. Ser. A* **1995**, 116 (2), 215–220.
- (28) Kentgens, A. P. M. A Practical Guide to Solid-State NMR of Half-Integer Quadrupolar Nuclei with Some Applications to Disordered Systems. *Geoderma* **1997**, 80 (3–4), 271–306.
- (29) Amoureux, J. P.; Fernandez, C.; Steuernagel, S. Z Filtering in MQMAS NMR. *Journal of Magnetic Resonance - Series A*. *J Magn Reson A* 1996, pp 116–118.
- (30) van Meerten, S. G. J.; Franssen, W. M. J.; Kentgens, A. P. M. SsNake: A Cross-Platform Open-Source NMR Data Processing and Fitting Application. *J. Magn. Reson.* **2019**, 301, 56–66.
- (31) Pickard, C. J.; Mauri, F. All-Electron Magnetic Response with Pseudopotentials: NMR Chemical Shifts. *Phys. Rev. B* **2001**, 63 (24), 245101.
- (32) Yates, J. R.; Pickard, C. J.; Mauri, F. Calculation of NMR Chemical Shifts for Extended Systems Using Ultrasoft Pseudopotentials. *Phys. Rev. B* **2007**, 76 (2), 24401.
- (33) Clark, S. J.; Segall, M. D.; Pickard, C. J.; Hasnip, P. J.; Probert, M. I. J.; Refson, K.; Payne, M. C. First Principles Methods Using CASTEP. *Zeitschrift für Krist.* **2005**, 220 (5–6), 567–570.
- (34) Perdew, J. P.; Burke, K.; Ernzerhof, M. Generalized Gradient Approximation Made Simple. *Phys. Rev. Lett.* **1996**, 77 (18), 3865–3868.
- (35) Haeberlen, U. *High Resolution NMR in Solids : Selective Averaging*; Academic Press, 1976.

- (36) Tomas, A.; Pardo, M. P.; Guittard, M.; Guymont, M.; Famery, R. Determination Des Structures Des Formes α et β de Ga₂S₃ Structural Determination of α and β Ga₂S₃. *Mater. Res. Bull.* **1987**, 22 (11), 1549–1554.
- (37) Noi, K.; Hayashi, A.; Tatsumisago, M. Structure and Properties of the Na₂S–P₂S₅ Glasses and Glass–Ceramics Prepared by Mechanical Milling. *J. Power Sources* **2014**, 269, 260–265.
- (38) Casas-Cabanas, M.; Reynaud, M.; Rikarte, J.; Horbach, P.; Rodríguez-Carvajal, J. FAULTS: A Program for Refinement of Structures with Extended Defects. *J. Appl. Crystallogr.* **2016**, 49 (6), 2259–2269.
- (39) Kitamura, M.; Asano, A. Temperature Distribution in a Solid State NMR Sample Rotor during MAS Experiments. *Anal. Sci.* **2013**, 29 (11), 1089–1093.
- (40) Eisenmann, B.; Hofmann, A. Crystal Structure of Hexasodium Di- μ -Thiobis(Dithiogallate) — I, Na₆Ga₂S₆. *Zeitschrift für Krist. - Cryst. Mater.* **2014**, 197 (1–4), 143–144.
- (41) Eisenmann, B.; Hofmann, A. Crystal Structure of Hexasodium Di- μ -Thio-Bis(Dithiogallate) – II, Na₆Ga₂S₆. *Zeitschrift für Krist.* **1991**, 197 (1–2), 147–148.
- (42) Balijapelly, S.; Sandineni, P.; Adhikary, A.; Gerasimchuk, N. N.; Chernatynskiy, A. V.; Choudhury, A. Ternary Alkali Ion Thiogallates, A₅GaS₄ (A = Li and Na), with Isolated Tetrahedral Building Units and Their Ionic Conductivities . *Dalt. Trans.* **2021**, 50 (21), 7372–7379.

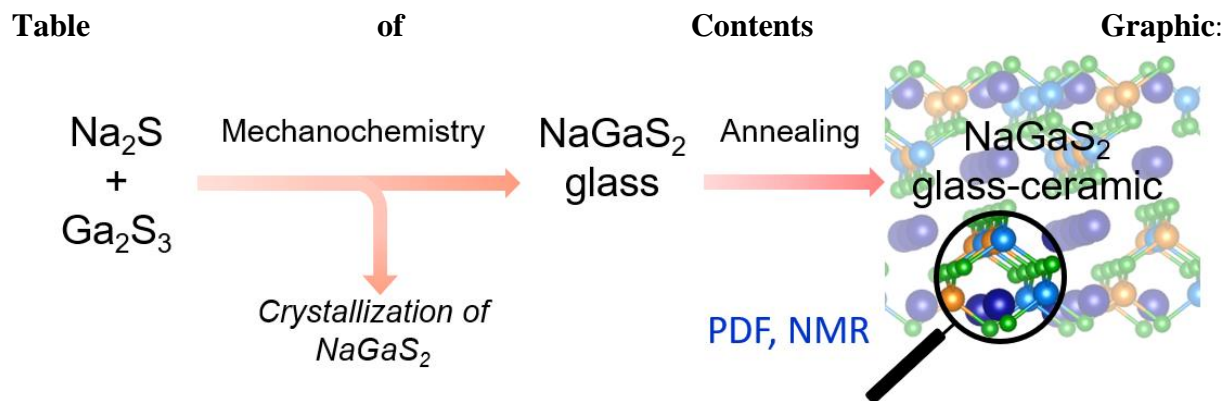


Table of Contents Synopsis:

NaGaS_2 has been synthesized by an alternative method to what has been previously published, namely by mechanochemistry, either by a direct one-step process, or by a two-step process. In the one-step process, crystalline NaGaS_2 is directly formed by milling sodium sulfide Na_2S and gallium (III) sulfide Ga_2S_3 . In the two-step process, amorphous NaGaS_2 is firstly obtained by mechanical milling, and then annealed to obtain a glass-ceramic mainly composed of crystalline NaGaS_2 .